

Relativistic plane wave predictions of polarization transfer observables for $(\vec{p}, 2\vec{p})$ knockout reactions from the $3s_{1/2}$ state in ^{208}Pb at 392 MeV

T. Mello^{1,*}, G. C. Hillhouse¹, and J. P. W. Diener¹

¹*Department of Physics and Astronomy, Botswana International University of Science and Technology (BIUST), Private Bag 16, Palapye, Botswana*

Background: Exclusive $(\vec{p}, 2\vec{p})$ reactions are often described within the Relativistic Distorted Wave Impulse Approximation (RDWIA) model, which incorporates potentials responsible for nuclear distortion effects. The Relativistic Plane Wave Impulse Approximation (RPWIA) model, on the other hand, neglects these effects on the incident and outgoing proton wave functions.

Purpose: To identify kinematic regions where the RPWIA model quantitatively describes energy-sharing analyzing power (A_y) and qualitatively describes the corresponding unpolarized triple differential cross section (σ) data. Where no data exist, we also seek regions where the RPWIA gives similar results of the complete set of polarization transfer observables ($D_{i'j}$) compared to the RDWIA model. The sensitivity of the RPWIA predictions to different Relativistic Mean Field (RMF) models (QHDII, NL3, FSUGold, FSUGold2) will be assessed.

Methods: For an incident proton beam with a kinetic energy of 392 MeV, and coplanar scattering angles, $\theta_{a'} = 32.5^\circ$ and $\theta_{b'} = -50.0^\circ$, the RPWIA predictions of σ and A_y are compared to published data for $(\vec{p}, 2\vec{p})$ knockout from the $3s_{1/2}$ state in ^{208}Pb . In the RPWIA model, the proton wave functions are treated as Dirac plane waves, the nucleon-nucleon (NN) interaction is modeled using the relativistic IA1 parameterization within the Relativistic Impulse Approximation (RIA) framework, and the boundstate wave functions are extracted from the above RMF models.

Results: Within a range of about ± 10 MeV around the peak of σ (corresponding to zero recoil momentum), both the RPWIA and the RDWIA models quantitatively describe the A_y data and qualitatively describes σ . In this range, the RPWIA and RDWIA predictions are in close agreement for all $D_{i'j}$. While σ is sensitive to the choice of the RMF model applied, the $D_{i'j}$ are insensitive to different RMF models.

Conclusions: The RPWIA model can be applied to provide a quantitative description of $D_{i'j}$ within a limited kinematic range for proton knockout from the $3s_{1/2}$ state in ^{208}Pb , and qualitatively describe the shape of σ .

I. INTRODUCTION

The study of nuclear reactions with polarized beams provides unique insights into the structure and dynamics of atomic nuclei. In particular, exclusive $(\vec{p}, 2\vec{p})$ reactions on stable nuclei have proven to be an invaluable tool to understand reaction mechanisms, determine the momentum distribution of nucleons in single-particle states in nuclei, extract spectroscopic factors, and investigate the influence of the nuclear medium on the free nucleon-nucleon (NN) interaction [1–6]. These reactions deploy an incident polarized proton beam to knockout protons from single-particle states in target nuclei, whereby the two scattered protons are detected in coincidence, with one of the protons being polarized [2, 7–9].

Compared to the more commonly measured energy-sharing unpolarized triple differential cross section distributions (which we refer to as cross sections for simplicity), complete sets of polarization transfer observables offer extremely stringent tests of theoretical models, with certain polarization transfer observables being more sensitive to specific model ingredients.

Eventually, the success of a particular model should be judged on its ability to simultaneously predict cross sections and complete sets of polarization transfer observables. Indeed, it is important to develop reliable predictive models for nuclear reactions on stable nuclei which could be extended to studies on unstable nuclei. Several key laboratories are currently under construction or have recently been upgraded to explore the properties of short-lived proton-rich and neutron-rich nuclei far from the line of stability, including the Facility for Antiproton and Ion Research (FAIR) in Germany, the Radioactive Ion Beam Facility (RIBF) in Japan, and the Facility for Rare Isotope Beams (FRIB) in the USA. The latter facilities could perform exclusive $(\vec{p}, 2\vec{p})$ reactions using inverse kinematics with unstable heavy-ion beams on polarized hydrogen targets [10–13].

The most extensive data sets for exclusive $(\vec{p}, 2\vec{p})$ reactions have been measured at the Research Center for Nuclear Physics (RCNP) in Japan, where both cross sections and analyzing power data were measured at an incident energy of 392 MeV on spherical target nuclei, ^{12}C , ^{16}O , ^{40}Ca and ^{208}Pb , leading to several single-particle states of the residual nuclei [3]. These measurements represent the best published data for testing the predictive power of exclusive $(\vec{p}, 2\vec{p})$ reaction models. The 392 MeV data have been mostly interpreted within the frameworks of the Non-Relativistic Distorted

* MT17000947@biust.ac.bw

Wave Impulse Approximation (NRDWIA) [3, 5, 6] and the Relativistic Distorted Wave Impulse Approximation (RDWIA) [3, 5, 6]. In both NRDWIA and RDWIA models, all kinematic quantities are fully relativistic, and the transition matrix elements have been modelled within the Relativistic Impulse Approximation (RIA) [14] which represents the free NN scattering amplitudes in terms of five Fermi (scalar, vector, pseudoscalar, axial-vector, and tensor) invariants, the so-called IA1 representation.

Within the framework of the NRDWIA model, the distorted wave functions are obtained by solving the non-relativistic Schrödinger equation through a transformation of relativistic scalar and vector optical potentials to Schrödinger-equivalent central and spin-orbit optical potentials. The relativistic scalar and vector optical potentials can be obtained from phenomenological parameterizations [7, 15–17] that are calibrated with respect to elastic scattering data or within the context of optical potentials that are obtained by folding the IA1 representation of the NN interaction with scalar and vector densities for the QHDII RMF model [18], the parameters of which have been calibrated with respect to the properties of infinite nuclear matter. The non-relativistic boundstate radial wave functions are extracted from the upper-component of the relativistic radial wave functions (thus neglecting the lower component radial wave functions) for the QHDII parameterization of a Relativistic Mean Field (RMF) model. Hence, the NRDWIA predictions represent a blend of both non-relativistic Schrödinger and relativistic Dirac aspects.

The RDWIA model, on the other hand, generates distorted wave functions by solving the relativistic Dirac equation for phenomenological or microscopic scalar and vector optical potentials. In contrast to the NRDWIA model, all of the RDWIA ingredients are fully relativistic. Although phenomenological and microscopic optical potentials provide reasonable descriptions of complete sets of elastic scattering proton-nucleus scattering observables at energies between 200 and 500 MeV [6, 19], the different potentials yield different quantitative values for $(\vec{p}, 2\vec{p})$ cross section distributions, thus yielding different values for the spectroscopic factors (which are obtained by normalizing the distorted wave cross sections to the experimental data) of single-particle states from which protons are knocked out [3]. Spectroscopic factors are related to occupation numbers of single-particle states, and the values range from 0.65 to 1.65 for the $3s_{1/2}$ state in ^{208}Pb depending on the choice of the optical potential [3, 6, 20].

The RDWIA model fully incorporates relativistic dynamics and kinematics, which allows for a proper description of the cross section and the analyzing power data of the $3s_{1/2}$ state in ^{208}Pb . This model also yields

reliable spectroscopic factors that are similar to the ones obtained from $(e, e'p)$ reactions [3, 6]. The distorted wave models (RDWIA and NRDWIA) incorporate optical potentials, which tend to bring about ambiguities in the overall interpretation of the polarization transfer observables [3]. Therefore, we need a model that does not rely on optical potentials to describe the cross section and analyzing power data.

Previous studies by Hillhouse and Noro demonstrate that, within certain kinematic regions, that is, near minimum recoil momentum, the analyzing power for the $(\vec{p}, 2\vec{p})$ reactions can be reproduced by applying the Relativistic Plane Wave Impulse Approximation (RPWIA) model [2, 3, 7]. Their results suggest that there is a window in which distortion effects become negligible. Motivated by these findings, this current work seeks to investigate whether this agreement can extend to the complete set of polarization transfer observables, which would provide a simple framework that does not rely on optical potentials for disentangling nuclear structure effects from reaction dynamics.

In this paper, we identify kinematic regions in the energy-sharing distributions of complete sets of $(\vec{p}, 2\vec{p})$ polarization transfer observables which are insensitive to distorting effects from different types of optical potentials. These results will inform future experiments of $(\vec{p}, 2\vec{p})$ reactions using inverse kinematics for unstable target nuclei where the availability of elastic scattering data to constrain optical potentials is limited or not available. For the identified regions where the RPWIA results quantitatively describe analyzing power data, results will also be compared to the RDWIA results.

The RPWIA model is applied for predictions of the unpolarized triple differential cross sections and the complete set of polarization transfer observables for the $3s_{1/2}$ state in ^{208}Pb . These predictions are compared with data from RCNP by Noro *et al.*, who measured the unpolarized triple differential cross sections and the analyzing powers of various stable spherical target nuclei and single-particle states using incident proton energy beams of 392 MeV and with coplanar scattering angles ($\theta_{a'} = 32.5^\circ$ and $\theta_{b'} = -50.0^\circ$) [3].

The $3s_{1/2}$ state is of interest because it has the highest peak of the unpolarized triple differential cross section compared to other single-particle states and its separation energy is well-isolated in the energy spectrum, allowing for an easier identification of the state. Additionally, for the $s_{1/2}$ state, the differential cross section achieves its maximum at zero recoil [9, 21]. The reaction mechanism is expected to be less complicated compared to states with higher angular momentum quantum numbers ($l \neq 0$).

The RPWIA predictions for the complete set of polarization transfer observables will be compared with the RDWIA predictions of Refs. [7, 19] for the range of outgoing proton energies around ± 10 MeV of the absolute peak of the unpolarized triple differential cross section: the energy range where the RPWIA show good agreement with the experiment data of the cross section. The RPWIA model formalism is presented in Sec. II with the relativistic scattering wave functions and the relativistic boundstate proton wave functions given in Sec. IIB and Sec. IIC respectively. The NN interaction between the incident proton and the bound proton inside the target nucleus is discussed in Sec. IID. Sec. III presents the expressions of the polarization transfer observables and the unpolarized triple differential cross section. The results, discussions and conclusions are given in Secs. IV, V and VI respectively.

II. RELATIVISTIC PLANE WAVE IMPULSE APPROXIMATION

In this section, the RPWIA model is described. The exclusive polarized proton-induced proton-knockout reaction $(\vec{p}, 2\vec{p})$, is a nuclear reaction in which a polarized projectile proton beam knocks out a proton from the target nucleus and the two outgoing protons are detected in coincidence [19, 22].

A. Notation

For a $(\vec{p}, 2\vec{p})$ knockout reaction, illustrated in Fig. 1, an incident polarized proton beam, a , with momentum \vec{k}_a , collides with a stationary target nucleus $A = C + b$, knocking out a bound proton, b , from a specific single-particle state [3, 7]. The outgoing protons, a' and b' , with momenta $\vec{k}_{a'}$ and $\vec{k}_{b'}$ respectively, are detected at coplanar scattering angles $\theta_{a'}$ and $\theta_{b'}$. This reaction leaves behind the residual nucleus (C) with a single-proton hole state which is characterized by quantum numbers, nlj , whereby the nlj represent the single-particle states of the target nucleus A [22]. The principal quantum number is denoted by n , the orbital angular momentum quantum number by l and the nuclear spin is represented by $j = l \pm \frac{1}{2}$. An alternative

notation style for the single-particle or single-proton hole state in the nucleus is denoted as j^π , whereby $\pi = (-1)^l$ represents the intrinsic parity of the single-particle state. These notation styles (nlj or j^π) are frequently used interchangeably in the context of $(\vec{p}, 2\vec{p})$ knockout reactions [3, 4].

The kinematic quantities of the incident and outgoing protons - the momenta k_i and energies E_i (with $i \in \{a, A, a', b', C\}$) are defined in terms of the rest masses m_i , the laboratory kinetic energies of the incoming and scattered protons (T_a and $T_{a'}$, respectively), the laboratory scattering angles ($\theta_{a'}$ and $\theta_{b'}$) and the excitation energy of the ejected proton from the target nucleus A [9]. Throughout this work, we will adopt natural units, i.e., $\hbar = c = 1$, unless stated otherwise. The kinematics and polarization transfer observables can be expressed via orthogonal coordinate systems within the laboratory frames of incident $(\hat{\ell}, \hat{n}, \hat{s})$ and ejected protons $(\hat{\ell}', \hat{n}', \hat{s}')$ [19]:

$$\begin{aligned}\hat{\ell} &= \hat{z} = \hat{k}_a, & \hat{n} &= \hat{y} = \hat{k}_a \times \hat{k}_{a'}, \\ \hat{s} &= \hat{x} = \hat{n} \times \hat{\ell}, & \hat{\ell}' &= \hat{z}' = \hat{k}_{a'}, \\ \hat{n}' &= \hat{n} = \hat{y}, & \hat{s}' &= \hat{x}' = \hat{n} \times \hat{\ell}'.\end{aligned}\tag{1}$$

The $(\vec{p}, 2\vec{p})$ scattering observables are obtained through the use of the transition amplitude, $T_{ljm_j}(s_a, s_{a'}, s_{b'})$, which incorporates the details of the initial and final state of the reaction, and is given by [2, 7, 9, 23]:

$$\begin{aligned}T_{ljm_j}(s_a, s_{a'}, s_{b'}) &= \\ &\int d^3\vec{x} [\bar{\psi}^{(-)}(\vec{x}, \vec{k}_{a'}, s_{a'}) \otimes \bar{\psi}^{(-)}(\vec{x}, \vec{k}_{b'}, s_{b'})] \\ &\times \hat{F}[\psi^{(+)}(\vec{x}, \vec{k}_a, s_a) \otimes \phi_{ljm_j}(\vec{x})],\end{aligned}\tag{2}$$

where the wave function of the incident proton is represented as $\psi^{(+)}(\vec{x}, \vec{k}_a, s_a)$, while the wave functions of the scattered protons are denoted as $\bar{\psi}^{(-)}(\vec{x}, \vec{k}_{a'}, s_{a'})$ and $\bar{\psi}^{(-)}(\vec{x}, \vec{k}_{b'}, s_{b'})$, respectively. The four-component scattering wave functions are solutions to the free Dirac equation. The symbol \otimes denotes the Kronecker, the nucleon-nucleon (NN) interaction is represented by \hat{F} , and the relativistic proton bound state wave function by $\phi_{ljm_j}(\vec{x})$. We adopt RIA which assumes that the NN scattering matrix inside the nuclear medium is identical to that of free NN scattering.

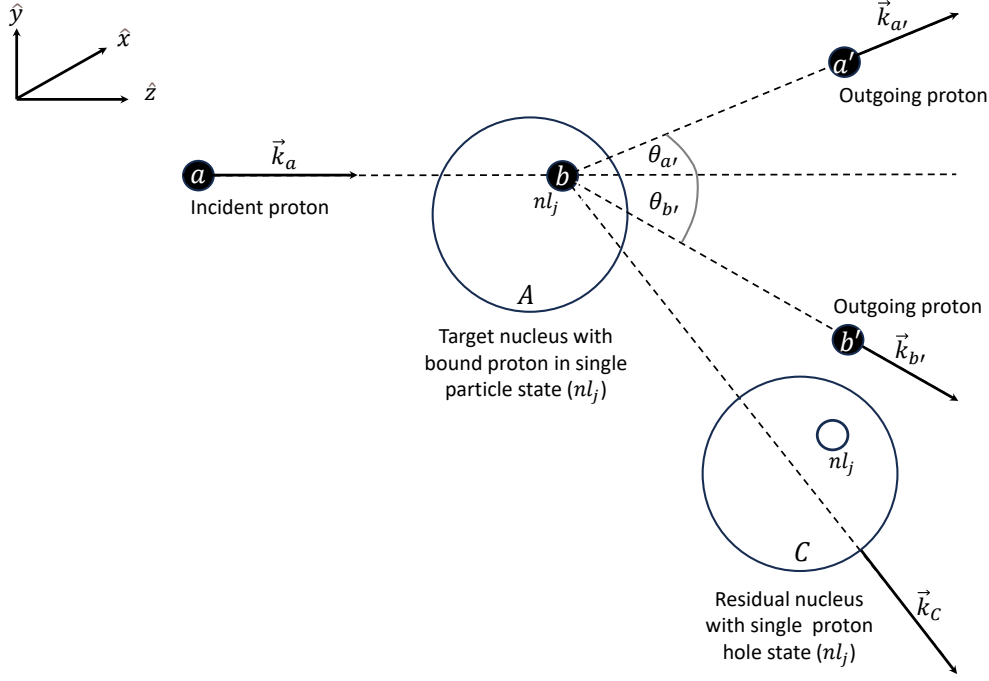


FIG. 1: Schematic illustration of a $(\vec{p}, 2\vec{p})$ knockout reaction: see the text for an explanation of the notation.

B. Relativistic scattering wave functions

The relativistic wave functions of protons, $\psi(\vec{x}, \vec{k}_i, s_i)$ where $i = a, a', b'$, are treated as relativistic Dirac plane waves [24]:

$$\begin{aligned}\psi^{(+)}(\vec{x}, \vec{k}_a, s_a) &= e^{i\vec{k}_a \cdot \vec{x}} U(\vec{k}_a, s_a), \\ \psi^{(-)}(\vec{x}, \vec{k}_{a'}, s_{a'}) &= e^{-i\vec{k}_{a'} \cdot \vec{x}} U(\vec{k}_{a'}, s_{a'}), \\ \psi^{(-)}(\vec{x}, \vec{k}_{b'}, s_{b'}) &= e^{-i\vec{k}_{b'} \cdot \vec{x}} U(\vec{k}_{b'}, s_{b'}).\end{aligned}\quad (3)$$

The four-component Dirac spinor, $U(\vec{k}_i, s_i)$ is given by:

$$U(\vec{k}_i, s_i) = \sqrt{\frac{E_i + m_i}{2m_i}} \begin{pmatrix} 1 \\ \vec{\sigma} \cdot \vec{k}_i \\ E_i + m_i \end{pmatrix} \chi_{s_i}, \quad (4)$$

where $\vec{\sigma}$ are the Pauli spin matrices and $\chi_{s_i=\pm\frac{1}{2}}$ are the Pauli spinors. The Dirac spinors are normalized such that $\bar{U}(\vec{k}_i, s_i)U(\vec{k}_i, s_i) = 1$. Substituting Eqs. (3) and (4) into Eq. (2) yields:

$$\begin{aligned}T_{ljm_j}(s_a, s_{a'}, s_b) &= \\ \int d^3\vec{x} [e^{-i\vec{k}_{a'} \cdot \vec{x}} \bar{U}(\vec{k}_{a'}, s_{a'}) \otimes e^{-i\vec{k}_{b'} \cdot \vec{x}} \bar{U}(\vec{k}_{b'}, s_{b'})] \\ \times \hat{F}[e^{i\vec{k}_a \cdot \vec{x}} U(\vec{k}_a, s_a) \otimes \phi_{ljm_j}(\vec{x})],\end{aligned}\quad (5)$$

The momentum of the residual nucleus is given by:

$$\vec{k}_C = \vec{k}_a - \vec{k}_{a'} - \vec{k}_{b'} = -\vec{K}. \quad (6)$$

Incorporating Eq. (6) into Eq. (5) results in the following expression:

$$\begin{aligned}T_{ljm_j}(s_a, s_{a'}, s_{b'}) &= [\bar{U}(\vec{k}_{a'}, s_{a'}) \otimes \bar{U}(\vec{k}_{b'}, s_{b'})] \\ \times \hat{F}[U(\vec{k}_a, s_a) \otimes \int d^3\vec{x} e^{-i\vec{K} \cdot \vec{x}} \phi_{ljm_j}(\vec{x})],\end{aligned}\quad (7)$$

Applying the relation:

$$\phi_{ljm_j}(\vec{K}) = \phi_{ljm_j}(-\vec{k}_C) = \int d^3\vec{x} e^{-i\vec{K} \cdot \vec{x}} \phi_{ljm_j}(\vec{x}). \quad (8)$$

to Eq. (7), leads to:

$$\begin{aligned}T_{ljm_j}(s_a, s_{a'}, s_{b'}) &= [\bar{U}(\vec{k}_{a'}, s_{a'}) \otimes \bar{U}(\vec{k}_{b'}, s_{b'})] \\ \times \hat{F}[U(\vec{k}_a, s_a) \otimes \phi_{ljm_j}(\vec{K})],\end{aligned}\quad (9)$$

C. Relativistic boundstate proton wave functions

The boundstate proton radial wave functions $\phi_{ljm_j}(\vec{x})$ are obtained via self-consistent solutions of the Dirac-Hartree field equations from Quantum Hadrodynamics (QHD) and application of RMF

approximation [25] discussed in Sec. II C 1.

The relativistic boundstate proton wave functions are given by [22]:

$$\phi_{ljm_j}(\vec{x}) = \frac{1}{x} \sum_{s_B} \left[u_{lj}(x) \langle l, m_j - s_B, \frac{1}{2}, s_B | j, m_j \rangle Y_{l, m_j - s_B}(\hat{x}) \chi_{s_B} + i w_{lj}(x) \langle 2j - l, m_j - s_B, \frac{1}{2}, s_B | j, m_j \rangle Y_{2j - l, m_j - s_B}(\hat{x}) \chi_{s_B} \right]. \quad (10)$$

where u_{lj} and w_{lj} represent the upper and lower proton radial wave functions, respectively, of the bound proton which are obtained through self-consistent solutions of the RMF equations, the spherical harmonics are denoted by Y , and the Clebsch-Gordon coefficients are represented by the brackets $\langle \rangle$. Eqs. (8) and (10) combine to give:

$$\phi_{ljm_j}(\vec{k}_C) = \left[\begin{array}{c} 4\pi i^l \mathcal{Y}_{ljm_j}(\theta_{k_C}, \phi_{k_C}) u_{lj}(k_C) \\ 4\pi i^{2j-l+1} \mathcal{Y}_{2j-l+1, j m_j}(\theta_{k_C}, \phi_{k_C}) w_{2j-l, j}(k_C) \end{array} \right], \quad (11)$$

where [22]:

$$u_{lj}(k_C) = \int_0^\infty dx x j_l(k_C x) u_{lj}(x), \\ w_{2j-l, j}(k_C) = \int_0^\infty dx x j_{2j-l}(k_C x) w_{lj}(x),$$

Thus, the relativistic proton boundstate wave function in Eq. (11) can be expressed as:

$$\phi_{ljm_j}(\vec{k}_C) = 4\pi \sum_{s'_z} \left[i^l u_{lj}(k_C) \langle l, \frac{1}{2}, m_j - s'_z, s'_z | j m_j \rangle Y_{l, m_j - s'_z}(\theta, \phi) \chi_{s'_z} + i^{2j-l+1} w_{2j-l, j}(k_C) \langle 2j - l, \frac{1}{2}, m_j - s'_z, s'_z | j m_j \rangle Y_{2j-l, m_j - s'_z}(\theta, \phi) \chi_{s'_z} \right]. \quad (13)$$

1. Lagrangian density

To extract the relativistic boundstate proton radial wave functions u_{lj} and w_{lj} , we use RMF models with the following interacting Lagrangian density [26–29]:

$$\mathcal{L}_{\text{int}} = \bar{\psi} \left[g_s \phi - \gamma^\mu (g_v V_\mu + \frac{g_\rho}{2} \boldsymbol{\tau} \cdot \mathbf{b}_\mu + \frac{e}{2} (1 + \tau_3) A^\mu) \right] \psi \\ - \frac{\kappa}{3!} (g_s \phi)^3 - \frac{\lambda}{4!} (g_s \phi)^4 + \frac{\zeta}{4!} (g_v^2 V^\mu V_\mu)^2 \\ + \Lambda_v (g_v^2 V^\mu V_\mu) (g_\rho^2 \mathbf{b}^\mu \cdot \mathbf{b}_\mu). \quad (14)$$

where ψ represents the iso-doublet baryon field, the isoscalar-scalar σ -, isoscalar-vector ω -, isovector-vector ρ - meson fields are represented by ϕ , V^μ , \mathbf{b}^μ , together with their coupling constants g_s , g_v and g_ρ respectively. The Dirac matrices are denoted by γ^μ , the photon field

by A^μ , and the isospin operator by $\boldsymbol{\tau}$. The other terms in Eq. (14) show different mixed and self-interactions of the various meson fields and their respective coupling strengths given by: κ , λ , ζ , and Λ_v [26–29]. For this study, we consider the following RMF models: QHDII [18], NL3 [26], FSUGold [27] and FSUGold2 [28], with the parameter sets given in Table I. QHDII and NL3 evolved from the original QHDI (so-called $\sigma - \omega$ model) parameter set [30]. The FSUGold model introduced the Λ_v coupling to improve the so-called breathing modes, the isoscalar giant monopole resonance (GMR) and the isovector giant dipole resonance (IVGDR) in ^{208}Pb [27]. FSUGold2 extends the FSUGold model with constraints from the properties of finite and infinite nuclear matter (neutron stars) [28]. All parameter sets of the different RMF models are calibrated to reproduce the properties of saturated nuclear matter: saturation density, binding energy, compressibility and symmetry energy [30].

TABLE I: The model parameters for the different RMF models: QHDII, NL3, FSUGold, and FSUGold2, obtained from Refs. [18, 26, 29, 31, 32]. The nucleon mass is fixed at $M = 939$ MeV.

Model	m_s	m_v	m_ρ	g_s^2	g_v^2	g_ρ^2	κ	λ	ζ	Λ
QHDII	520.0	783.0	770.0	109.6	190.4	65.2	0.0000	0.000 000	0.0000	0.000 000
NL3	508.2	782.5	763.0	104.4	165.6	79.6	3.8599	-0.015 905	0.0000	0.000 000
FSUGold	491.5	782.5	763.0	112.2	204.5	138.5	1.4203	0.023 762	0.0600	0.030 000
FSUGold2	497.5	782.5	763.0	108.1	183.8	80.5	3.0029	-0.000 533	0.0256	0.000 823

D. Nucleon-nucleon interaction

For the NN interaction (\hat{F}), we employ the IA1 representation [14, 33, 34] to Eq. (9) which yields:

$$T_{ljm_j}(s_a, s_{a'}, s_{b'}) = \sum_{i=S}^T F_i [\bar{U}(\vec{k}_{a'}, s_{a'}) \otimes \bar{U}(\vec{k}_{b'}, s_{b'})] \times [\lambda^i \otimes \lambda_i] [U(\vec{k}_a, s_a) \otimes \phi_{ljm_j}(\vec{k}_C)], \quad (15)$$

where λ_i 's represents the five Dirac matrices (1, $\gamma_\mu, \gamma_5, \gamma_5 \gamma_\mu, \sigma_{\mu\nu}$) given in Table II. Using the identity:

$$(M_1 \otimes M_2)(M_3 \otimes M_4) = (M_1 M_3) \otimes (M_2 M_4), \quad (16)$$

whereby M_j for $j \in \{1, 2, 3, 4\}$ represents the $4 \otimes 1$ matrices, gives:

$$T_{ljm_j}(s_a, s_{a'}, s_{b'}) = \sum_{i=S}^T F_i [\bar{U}(\vec{k}_{a'}, s_{a'}) \lambda_1^i U(\vec{k}_a, s_a)] \otimes [\bar{U}(\vec{k}_{b'}, s_{b'}) \lambda_{2i} \phi_{ljm_j}(\vec{k}_C)]. \quad (17)$$

Since $\bar{U}(\vec{k}_{a'}, s_{a'}) \lambda_1^i U(\vec{k}_a, s_a)$ are complex numbers, one can write Eq. (17) as:

$$T_{ljm_j}(s_a, s_{a'}, s_{b'}) = \sum_{i=S}^T F_i [\bar{U}(\vec{k}_{a'}, s_{a'}) \lambda_1^i U(\vec{k}_a, s_a)] \times [\bar{U}(\vec{k}_{b'}, s_{b'}) \lambda_{2i} \phi_{ljm_j}(\vec{k}_C)]. \quad (18)$$

The NN interaction from Eq. (2), \hat{F} , is evaluated using the effective laboratory kinetic energy and centre of mass scattering angles based on the final energy prescription [9] and is given by [35–38]:

$$\hat{F} = \sum_{i=S}^T F_i (\lambda^{i(1)} \cdot \lambda_{i(2)}) \quad (19)$$

where the superscripts (1) and (2) represent the incident and target nucleons, respectively. The i 's denote the five Dirac matrices listed in Table (II) and the contraction of the Lorentz indices is shown by the dot product.

TABLE II: The Dirac matrices of SVPAT.

i	λ_i
S (Scalar)	I_4
V (Vector)	γ_μ
P (Pseudoscalar)	γ_5
A (Axial-vector)	$\gamma_5 \gamma_\mu$
T (Tensor)	$\sigma_{\mu\nu}$

III. POLARIZATION TRANSFER OBSERVABLES

The development of polarized ion sources and high-resolution spectrometers with polarimeters has led to the study of exclusive $(\vec{p}, 2\vec{p})$ polarization transfer observables [3, 4, 37]. While measurements of the unpolarized triple differential cross section have been sufficient in terms of providing information about the structure of nuclei, different polarization transfer observables are selectively sensitive to specific model ingredients of the reaction [19]. These observables, $D_{i'j}$, are related to the probability that an incident polarized proton beam with initial spin orientation j will change into a final spin projection i' [22]. The unpolarized triple differential cross section is given by [19, 22]:

$$\sigma = \frac{d^3\sigma}{dT_{a'} d\Omega_{a'} d\Omega_b} = S_{lj} \sigma_{\text{calc}}, \text{ with} \quad (20)$$

$$\sigma_{\text{calc}} = \frac{F_{kin}}{(2s_a + 1)(2j + 1)} \sum_{m_j, s_b} \text{Tr}(TT^\dagger), \quad (21)$$

where S_{lj} represents the spectroscopic factor related to the single-particle state occupation numbers and F_{kin} is a kinematic factor given by [19, 39]:

$$F_{kin} = \frac{E_a E_{a'} E_b}{(2\pi)^5} \frac{k_{a'} k_b}{k_a} \times \left[1 + \frac{E_b}{E_C} \left(1 - \frac{k_a}{k_b} \cos \theta_b + \frac{k_{a'}}{k_b} \cos(\theta_{a'} + \theta_b) \right) \right]^{-1}. \quad (22)$$

The polarization transfer observables, $D_{i'j}$, are defined as [19, 22]:

$$D_{i'j} = \frac{\text{Tr}(T\sigma_j T^\dagger \sigma_{i'})}{\text{Tr}(TT^\dagger)}, \quad (23)$$

where the 2×2 Pauli spin matrices are given by:

$$\begin{aligned} \sigma_0 &= \begin{pmatrix} 1 & 0 \\ 0 & 1 \end{pmatrix}, & \sigma_{\hat{x}} &= \sigma_{\hat{s}} = \sigma_{\hat{s}'} = \begin{pmatrix} 0 & 1 \\ 1 & 0 \end{pmatrix}, \\ \sigma_{\hat{y}} &= \sigma_{\hat{n}} = \begin{pmatrix} 0 & -i \\ i & 0 \end{pmatrix}, & \sigma_{\hat{z}} &= \sigma_{\hat{\ell}} = \sigma_{\hat{\ell}'} = \begin{pmatrix} 1 & 0 \\ 0 & -1 \end{pmatrix}, \end{aligned} \quad (24)$$

The analyzing power is denoted as A_y ($D_{0'n}$), induced polarization by P ($D_{n'0}$), and other polarization transfer observables by $D_{n'n}$, $D_{s'\ell}$, $D_{s's}$, $D_{\ell's}$ and $D_{\ell'\ell}$ [7]. For polarization transfer observables, the spectroscopic factor S_{lj} cancels in the numerator and denominator of Eq. (23). T is a 2×2 matrix given by [7, 9]:

$$T = \begin{pmatrix} T_{lj}^{s_a=+\frac{1}{2}, s_{a'}=+\frac{1}{2}} & T_{lj}^{s_a=-\frac{1}{2}, s_{a'}=+\frac{1}{2}} \\ T_{lj}^{s_a=-\frac{1}{2}, s_{a'}=+\frac{1}{2}} & T_{lj}^{s_a=-\frac{1}{2}, s_{a'}=-\frac{1}{2}} \end{pmatrix}, \quad (25)$$

where s_a and $s_{a'}$ denote the spin projections of the incident (a) and outgoing (a') protons respectively. To preserve time-reversal, parity and rotational invariance to the NN scattering matrix, only seven polarization transfer observables are allowed: $D_{n'0}$, $D_{0'n}$, $D_{n'n}$, $D_{s'\ell}$, $D_{s's}$, $D_{\ell's}$ and $D_{\ell'\ell}$ [40]. The matrix elements $T_{lj}^{s_a, s_{a'}}$ are associated with the relativistic $(\vec{p}, 2\vec{p})$ transition matrix element $T_{lj m_j}(s_a, s_{a'}, s_b)$ through [9, 19, 22]:

$$T_{lj}^{s_a, s_{a'}} = \sum_{m_j, s_b} T_{lj m_j}(s_a, s_{a'}, s_b). \quad (26)$$

IV. RESULTS

In this section, we present our results. We first provide the single-particle proton energies extracted from different RMF parameterizations, together with the relativistic boundstate proton radial wave functions. The emphasis is on the predictions of the RPWIA energy-sharing unpolarized triple differential cross sections and the analyzing power, which are compared

with the available experimental data. Furthermore, we present the complete set of polarization transfer observables and compare them with the corresponding RDWIA calculations. Finally, we investigate the sensitivity of polarization transfer observables to the choice of RMF parameterization.

The results for the single-particle proton energies are presented in Table III, relativistic boundstate proton radial wave functions in Fig. 2, the unpolarized triple differential cross sections and the complete set of polarization transfer observables in Fig. 3 for knockout from the $3s_{1/2}$ state in ^{208}Pb .

A. Single-particle proton energies

We start by providing the results for the single-particle proton energies of the $3s_{1/2}$ state in ^{208}Pb for different RMF models compared to the experimental data of Refs. [3, 39, 41] presented in Table III. The QHDII model underpredicts the data by -2.1 MeV, NL3 yields the same result as the experimental data while the FSUGold and FSUGold2 models are within 0.1 MeV. Although FSUGold2 deviates from the experimental data by 0.1 MeV, it shows that it still yields a desirable result for the single-particle proton energy of the $3s_{1/2}$ state. However, a definitive assessment of the “best” RMF model needs consistency across other observables beyond the single-particle energies. We proceed to present the results of the relativistic boundstate wave functions in Sec. IV B.

B. Relativistic boundstate proton wave functions

For this section, we present results of the upper and lower components of the relativistic boundstate proton radial wave functions in Fig. 2. Fig. 2(a), represents the upper component of the proton radial wave function and the corresponding lower components on Fig. 2(b) for the $3s_{1/2}$ in ^{208}Pb . The upper components have larger amplitudes than the lower component radial wave functions, which implies that the significant contribution to the boundstate proton wave functions comes from the upper components.

TABLE III: Comparison of the single-particle proton energies (MeV) from various RMF models with data from Refs. [3, 39, 41] and the $3s_{1/2}$ single-particle state of ^{208}Pb .

Target nucleus	State (n_{lj})	Experiment	QHDII	NL3	FSUGold	FSUGold2
^{208}Pb	$3s_{1/2}$	-8.0	-5.9	-8.0	-8.1	-8.1

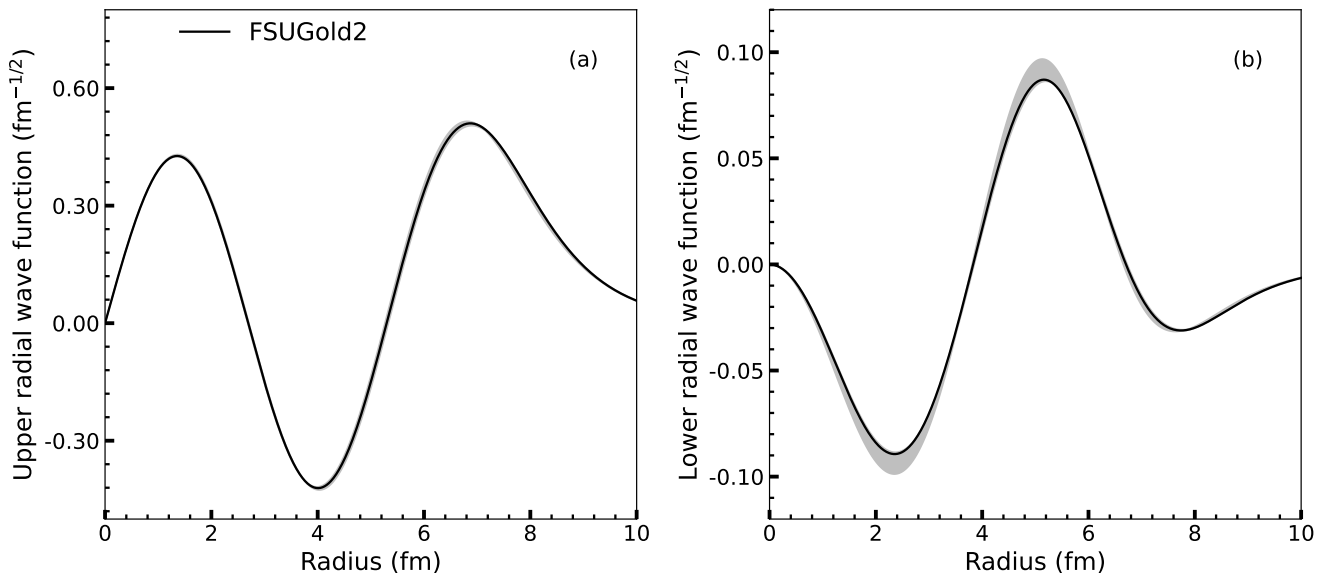


FIG. 2: The $3s_{1/2}$ state of ^{208}Pb upper and lower proton radial wave functions as functions of the nuclear radius (fm). The left panel represents the upper proton radial wave functions, while the right panel show the lower proton radial wave functions for various RMF models: QHDII, NL3, FSUGold, and FSUGold2. The solid black line shows the FSUGold2 model, while the gray shaded band contains the collective variation and the other models (QHDII, NL3, and FSUGold).

C. Cross section and polarization transfer observables

In this particular section, we present the results of the energy-sharing unpolarized triple differential cross sections and complete set of polarization transfer observables, as shown in Fig. 3. RPWIA predictions of cross sections and the analyzing power are compared with experimental data from RCNP from Ref. [3]. Furthermore, the RPWIA predictions of other polarization transfer observables are compared with the RDWIA predictions of Hillhouse *et al.* in Ref. [7, 19]. These comparisons are made for incident proton energies of 392 MeV and at coplanar scattering angles ($\theta_{a'} = 32.5^\circ$ and $\theta_{b'} = -50.0^\circ$) applied to the $3s_{1/2}$ state of ^{208}Pb . The purpose of this study is threefold: first, to examine how well the RPWIA describes the energy-sharing cross sections and analyzing power data; second, to investigate

how the RPWIA calculations compare with the more sophisticated RDWIA calculations of other polarization transfer observables; and lastly, to investigate the sensitivity of the predictions to different RMF models (QHDII, NL3, FSUGold, and FSUGold2). These analysis will help in clarifying whether various choices of RMF parameterizations lead to distinct predictions of polarization transfer observables. Currently, there are no available data for the energy distributions of the complete set of polarization transfer observables.

Based on the predictions by Noro [3] and Hillhouse [2, 7] we focus on regions of ± 10 MeV around the energy corresponding to zero-recoil momentum, which corresponds to the peak of the cross section. In this region, we compare RPWIA and RDWIA predictions to analyzing power data (A_y) and to the other polarization transfer observables. Fig. 3 represents the results for the $3s_{1/2}$ state of ^{208}Pb from this work for the predictions of

the RPWIA model of the unpolarized triple differential cross sections and the complete set of polarization transfer observables as functions of the kinetic energy of the outgoing proton, $T_{a'}$ (MeV) for various RMF models. The unpolarized triple differential cross sections are shown in panel Fig. 3(a), the analyzing power (A_y) on panel Fig. 3(b), the induced polarization (P) and other polarization transfer observables on panels: Figs. 3(c) - (h).

V. DISCUSSION

We discuss the results of the RPWIA predictions of the unpolarized triple differential cross sections and the complete set of polarization transfer observables of the $3s_{1/2}$ state in ^{208}Pb .

A. Comparison of RPWIA predictions to data

The results of the RPWIA predictions are compared with the available data of the unpolarized triple differential cross sections (σ) and analyzing powers (A_y). For the single-particle state of interest, $3s_{1/2}$ of ^{208}Pb , the RPWIA model qualitatively describes the data for the unpolarized triple differential cross sections as we obtain the overall shape of the experimental data. The symmetric shape of the cross section is also observed in Fig. 3 for the $3s_{1/2}$ state. This feature is also seen in Refs. [3, 19]. The RPWIA predictions for the unpolarized triple differential cross sections were divided by 26 to fit the predictions to the data. The RPWIA model quantitatively describes the analyzing power (A_y) data for the $3s_{1/2}$ single-particle state in ^{208}Pb within our selected energy ranges for the kinetic

energy of the outgoing proton. Various RMF models investigated: QHDII, NL3, FSUGold, and FSUGold2 show little variations in the predictions of the unpolarized triple differential cross sections and analyzing powers.

B. Comparison of the RPWIA to RDWIA predictions

Data are not available for the complete set of polarization transfer observables. The RPWIA predictions are compared to the well-established RDWIA model predictions within our selected energy ranges, ± 10 MeV from the peak of the unpolarized triple differential cross section. For the $3s_{1/2}$ state, the RPWIA and RDWIA share intersection points at certain energy ranges for the outgoing proton kinetic energies for the observables: P, D_{nn} , $D_{\ell's}$, $D_{s'\ell}$, and $D_{\ell'\ell}$. More experimental data are needed to see how the RPWIA model will perform with regard to data.

C. Sensitivity of polarization transfer observables to RMF models

From Fig. 3, the unpolarized triple differential cross sections and the complete set of polarization transfer observables are shown for different RMF models (QHDII, NL3, FSUGold, and FSUGold2) for the proton knockout from the $3s_{1/2}$ state. The predictions from the RMF models show little variation in the RPWIA predictions of the unpolarized triple differential cross sections. The complete set of polarization transfer observables appear to be insensitive to the RMF models since they give the same predictions within our selected energy ranges. This implies that the choice of the RMF applied has a limited effect on the polarization transfer observables.

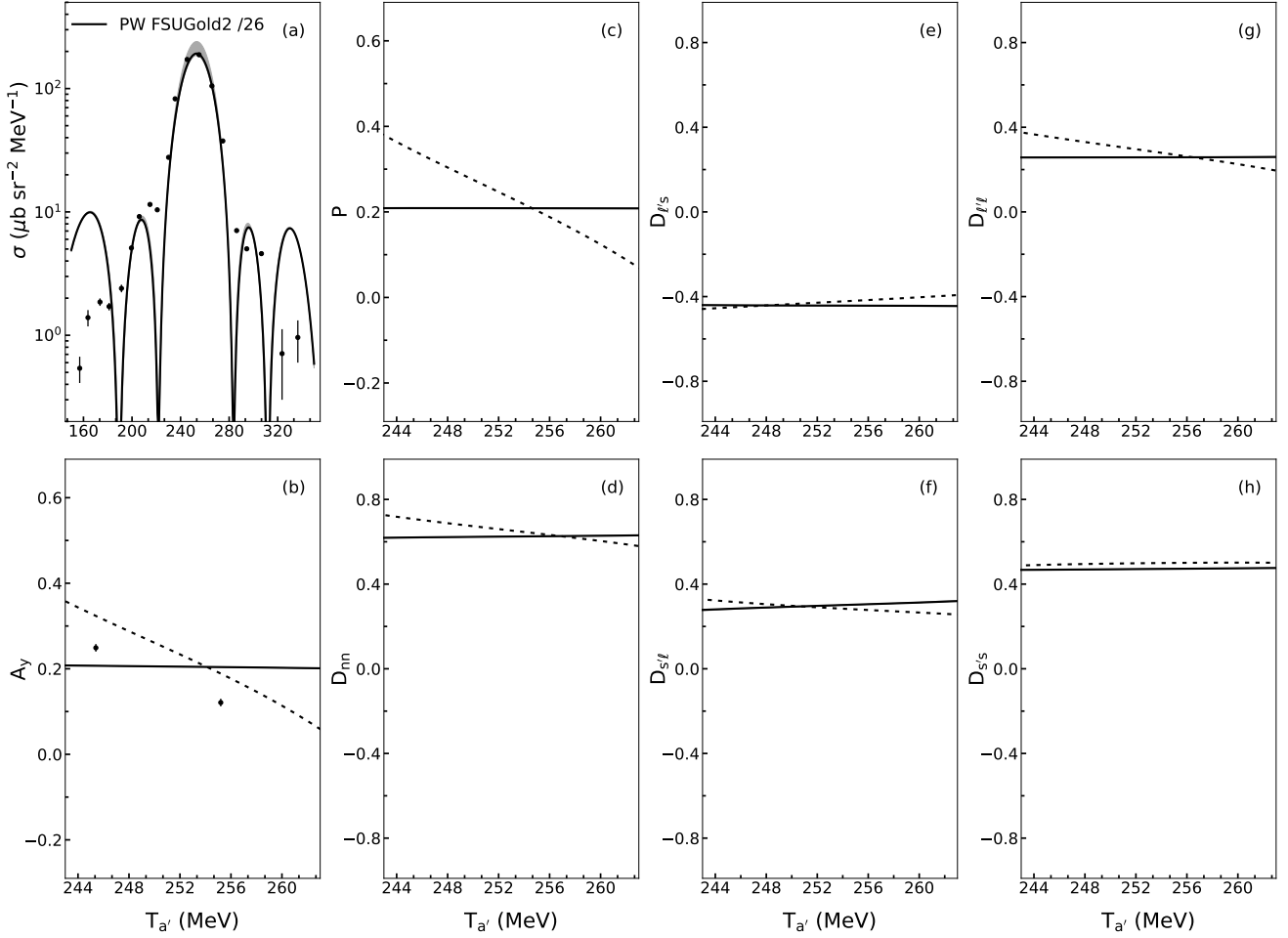


FIG. 3: The $3s_{1/2}$ state on ^{208}Pb unpolarized triple differential cross section, σ ($\mu\text{b sr}^{-2} \text{MeV}^{-1}$), analyzing power A_y and polarization transfer observables $D_{i'j}$, for proton knockout for incident proton energy of 392 MeV and coplanar scattering angles, $\theta_{a'} = 32.5^\circ$ and $\theta_{b'} = -50.0^\circ$, versus the kinetic energy of the outgoing proton [$T_{a'}$ (MeV)] for various RMF models: QHDII, NL3, FSUGold, and FSUGold2. The solid (dashed) black line represents the RPWIA (RDWIA) results for using the FSUGold2 RMF model for the $3s_{1/2}$ boundstate wave functions. The gray shaded band shows the collective variations in the RPWIA predictions of the RMF models for all observables of interest. The data are from Ref. [3].

VI. CONCLUSIONS

In this work, we applied the RPWIA model for the predictions of the unpolarized triple differential cross sections and the complete set of polarization transfer observables as functions of the energy of the outgoing proton, for $(\vec{p}, 2\vec{p})$ knockout reactions from the $3s_{1/2}$ state of ^{208}Pb . The predictions of the shape of the unpolarized triple differential cross sections and the analyzing powers were compared to experimental data of incident proton energy of 392 MeV and coplanar

scattering angles ($\theta_{a'} = 32.5^\circ$ and $\theta_{b'} = -50.0^\circ$) from RCNP [3]. Various RMF models: QHDII, NL3, FSUGold, and FSUGold2 were applied to investigate the sensitivity of polarization transfer observables to these different models.

The RPWIA model qualitatively describes the shape of the experimental data of the unpolarized triple differential cross section and also quantitatively describes the analyzing power data from RCNP for the $3s_{1/2}$ state in ^{208}Pb . The calculations of the complete set of polarization transfer observables were provided and compared with the RDWIA calculations. The RPWIA and the RDWIA calculations share intersection points, which implies that a “simple” model (RPWIA) which does not incorporate optical potentials and ignores the effects of distortions on the outgoing scattering wave functions can provide results similar to the sophisticated RDWIA model which relies on optical potentials. Within the region of interest, ± 10 MeV from the peak of the unpolarized triple differential cross section (corresponding to minimum recoil momentum), the complete set of polarization transfer observables are insensitive to investigated RMF models. Therefore, for as long as the RMF model is calibrated to reproduce the properties of infinite nuclear matter, it would suffice to extract the boundstate wave functions which are used in the calculations of the unpolarized triple differential cross sections and the complete set of polarization transfer observables. Future work will include a similar analysis for exclusive proton knockout from other

single-particle states in ^{208}Pb ($2d_{3/2}$, $1h_{11/2}$, $2d_{5/2}$ and $1g_{7/2}$).

Although the RPWIA model was applied to calculate the complete set of polarization transfer observables, these observables remain experimentally untested, which shows a gap that could guide future experimental work to measure these polarization transfer observables. Data are needed to fully validate the RPWIA model and extend our knowledge of polarization transfer observables in heavy nuclei, ^{208}Pb , and improve theoretical approaches of studying $(\vec{p}, 2\vec{p})$ knockout reactions which can then be extended to study atomic nuclei far from stability lines using inverse kinematics in the near future.

ACKNOWLEDGEMENT

The authors thank Prof. J. Piekarewicz for providing the code for extracting the RMF properties of infinite nuclear matter. TM acknowledges financial support from the Botswana International University of Science and Technology (BIUST) postgraduate funding, under grant number S00526.

-
- [1] N. S. Chant and P. G. Roos, Phys. Rev. C **27**, 1060 (1983).
 - [2] G. C. Hillhouse, J. Mano, A. A. Cowley, and R. Neveling, Phys. Rev. C **67**, 064604 (2003).
 - [3] T. Noro *et al.*, Prog. Theor. Exp. Phys **2020**, 093D02 (2020).
 - [4] T. Noro *et al.*, Prog. Theor. Exp. Phys **2023**, 093D01 (2023).
 - [5] R. Neveling, A. A. Cowley, G. F. Steyn, S. V. Förtsch, G. C. Hillhouse, J. Mano, and S. M. Wyngaardt, Phys. Rev. C **66**, 034602 (2002).
 - [6] T. Wakasa, K. Ogata, and T. Noro, Prog. Part. Nucl. Phys **96**, 32 (2017).
 - [7] G. C. Hillhouse, J. Mano, S. M. Wyngaardt, B. I. S. Van Der Ventel, T. Noro, and K. Hatanaka, Phys. Rev. C **68**, 034608 (2003).
 - [8] T. Mello, *Relativistic plane wave predictions of $(\vec{p}, 2\vec{p})$ polarization transfer observables on spherical nuclei*, Master’s thesis, BIUST (2025).
 - [9] G. C. Hillhouse and T. Noro, Phys. Rev. C **74**, 064608 (2006).
 - [10] T. Aumann, C. A. Bertulani, and J. Ryckebusch, Phys. Rev. C **88**, 064610 (2013).
 - [11] S. Chebotaryov *et al.*, Prog. Theor. Exp. Physics **2018**, 053D01 (2018).
 - [12] M. Patsyuk *et al.*, Nature Physics **17**, 693 (2021).
 - [13] S. Sakaguchi *et al.*, Phys. Rev. C **87**, 021601 (2013).
 - [14] C. J. Horowitz and D. P. Murdock, Phys. Rev. C **37**, 2032 (1988).
 - [15] E. D. Cooper, S. Hama, B. C. Clark, and R. L. Mercer, Phys. Rev. C **47**, 297 (1993).
 - [16] T. Ishida, *Experimental study of a relativistic effect through the $^{208}\text{Pb}(\vec{p}, 2p)^{207}\text{Tl}$ reaction at 392 MeV*, Ph.D. thesis, Kyushu University (2007).
 - [17] B. V. Overmeire, *A relativistic eikonal description of nucleon propagation through nuclei*, Ph.D. thesis, Universiteit Gent (2007).
 - [18] C. J. Horowitz, D. P. Murdock, and B. D. Serot, The relativistic impulse approximation, in *Computational Nuclear Physics 1: Nuclear Structure*, edited by K. Langanke, J. A. Maruhn, and S. E. Koonin (Springer Berlin Heidelberg, Berlin, Heidelberg, 1991) pp. 129–151.
 - [19] G. C. Hillhouse, T. Ishida, T. Noro, and B. Van Der Ventel, in *11th International Conference on Nuclear Reaction Mechanisms* (2006) pp. 23–32.
 - [20] A. Cowley, G. Arendse, J. Stander, and W. Richter, Phys. Lett. B **359**, 300 (1995).
 - [21] K. Hatanaka *et al.*, Phys. Rev. Lett. **78**, 1014 (1997).
 - [22] B. I. S. van der Ventel and G. C. Hillhouse, Phys. Rev. C **69**, 024618 (2004).
 - [23] T. Noro, *et al.*, Phys. Rev. C **77**, 044604 (2008).
 - [24] J. D. Bjorken and S. D. Drell, *Relativistic quantum mechanics*, International series in pure and applied physics (McGraw-Hill, New York, NY, 1964).
 - [25] B. D. Serot and J. D. Walecka, Recent Progress in Many-Body Theories , 49 (1992).
 - [26] G. A. Lalazissis, J. König, and P. Ring, Phys. Rev. C **55**, 540 (1997).
 - [27] B. G. Todd-Rutel and J. Piekarewicz, Phys. Rev. Lett. **95**, 122501 (2005).
 - [28] W. C. Chen and J. Piekarewicz, Phys. Rev. C **90**, 044305 (2014).

- [29] J. Piekarewicz, Phys. Rev. C **76**, 064310 (2007).
- [30] B. D. Serot and J. D. Walecka, International Journal of Modern Physics E **6**, 515 (1997).
- [31] B. G. Todd and J. Piekarewicz, Phys. Rev. C **67**, 044317 (2003).
- [32] J. Liu, Z. Ren, T. Dong, and Z. Sheng, Phys. Rev. C **84**, 064305 (2011).
- [33] C. J. Horowitz, Phys. Rev. C **31**, 1340 (1985).
- [34] C. J. Horowitz and B. D. Serot, Nucl. Phys. A **368**, 503 (1981).
- [35] J. A. McNeil, J. R. Shepard, and S. J. Wallace, Phys. Rev. Lett. **50**, 1439 (1983).
- [36] C. J. Horowitz and M. J. Iqbal, Phys. Rev. C **33**, 2059 (1986).
- [37] Y. Ikebata, Phys. Rev. C **52**, 890 (1995).
- [38] G. C. Hillhouse and P. R. De Kock, Phys. Rev. C **49**, 391 (1994).
- [39] J. Mano and Y. Kudo, Prog.Theor. Phys **100**, 91 (1998).
- [40] S. Wyngaardt, *Relativistic plane wave description of spin transfer observables for proton knock-out reactions*, Ph.D. thesis, Stellenbosch University (2001).
- [41] L. R. B. Elton and A. Swift, Nucl. Phys. A **94**, 52 (1967).